Journal of Solid State Chemistry 182 (2009) 3149–3154

Contents lists available at ScienceDirect

Journal of Solid State Chemistry

journal homepage: www.elsevier.com/locate/jssc

The effects of doping ferromagnetic spinel $CdCr_2Se_4$ with Sb^{3+} ions

E. Malicka [a], A. Waśkowska [b], D. Skrzypek [c], R. Sitko [a], D. Kaczorowski [b]

[a] Department of Chemistry, University of Silesia, Szkolna 9, 40-007 Katowice, Poland
[b] Institute of Low Temperature and Structure Research, Polish Academy of Sciences, P.O. Box 1410, 50-950 Wrocław, Poland
[c] A. Chełkowski Institute of Physics, University of Silesia, Uniwersytecka 4, 40-007 Katowice, Poland

ARTICLE INFO

Article history:
Received 10 May 2009
Received in revised form
31 August 2009
Accepted 6 September 2009
Available online 11 September 2009

Keywords:
Single crystals growth
X-ray diffraction
Magnetically ordered materials
Electron spin resonance
Magnetic measurements

ABSTRACT

Semiconducting spinel $CdCr_2Se_4$ orders ferromagnetically below T_C=130 K. A series of single-crystals of $CdCr_2Se_4$ doped with Sb^{3+} ions has been synthesized in order to study an effect of the substitution on the cation distribution and the magnetic properties. The compounds of $Cd_ySb_xCr_zSe_4$ have been investigated by means of X-ray diffraction, magnetization measurements and electron spin resonance spectroscopy. Two selected samples of the composition $(Cd_{1-x}Sb_x)[Cr_2]Se_4$ with x=0.13 and 0.44 retained cubic symmetry with space group $Fd\bar{3}m$. The unit cell parameter appeared to be sensitive to the concentration of Sb^{3+} admixture: it increases with x, despite a close similarity in the ionic radii of Cd^{2+} and Sb^{3+} in tetrahedral coordination. Upon partial substitution of Cd^{2+} by Sb^3 no obvious change in the Curie temperature was observed, however, the effective magnetic moment slightly increased, what may result from the appearance of Cr^{2+} ions. The characteristic feature of the system studied is an extended range of short-range magnetic order, in which the magnetic properties in the paramagnetic state are governed by the formation of ferromagnetic clusters, as indicated by both the bulk magnetometric and spectroscopic data.

1. Introduction

$CdCr_2Se_4$ belongs to the group of chalcogenide spinels that exhibit coexistence of long-range magnetic ordering and semiconductivity [1–7]. The magnetic behavior of this compound was first studied nearly 50 years ago, and already those investigations revealed its ferromagnetic nature below $T_C \approx 130$ K [1,3]. The paramagnetic Curie–Weiss temperature is as large as $\Theta_{C-W} \approx 200$ K, which indicates strong ferromagnetic exchange interactions. In the ordered state, the saturation magnetization was reported to be in the range 5.4–5.98 μ_B/mol [2,4], i.e. close to the value expected for the magnetic moments carried by Cr^{3+} ions. The electronic transport properties of $CdCr_2Se_4$ strongly depend on the actual stoichiometry and the presence of lattice defects in the specimens studied [8–11]. For example, it was observed that selenium vacancies cause the electrical conductivity to change from *n*- to *p*-type [7,11].

Since the spinel structure easily forms substitutional solid solutions, the interplay between magnetic and transport properties of $CdCr_2Se_4$ was also investigated by chemical substitution of non-magnetic Cd^{2+} or magnetic Cr^{3+} ions with various cations having different ionic radii and charge, e.g. with Ag^+, Ga^{3+} and In^{3+} [11–21]. It is well known that cation distribution is essential for the properties of spinels. It turned out that Ga^{3+} and In^{3+} ions can occupy both tetrahedral and octahedral sites in the spinel structure, while Ag^+ ions are always located in the tetrahedral sites [12,15]. For the compounds moderately diluted with Ga^{3+} and In^{3+} the long-range order remains as in the parent spinel, and only some decrease in the saturation magnetization was observed [16–21]. Only at high concentration of Ga^{3+} dopants ($x \approx 0.35$), a notable change in the magnetic behavior was observed, namely the ferromagnetic order was reported to turn into antiferromagnetism due to the formation of spin clusters in the ordered state [17,18].

In this work we communicate on the effect of diluting $CdCr_2Se_4$ with Sb^{3+} ions. A series of $Cd_ySb_xCr_zSe_4$ single crystals with nominal antimony concentration x, from 0.1 to 0.5, was grown. Recent studies on the crystal with x=0.25 have shown the *A*-site location of Sb^{3+} in the spinel structure, $(Cd_{1-x}Sb_x)[Cr_2]Se_4$, leading to the temperature dependent structural phase transition at 130 K [22] connected with lowering the crystal symmetry to orthorhombic space group *Fddd*. Although no observable impact on the magnetic transition temperature T_c was observed, a small increase in saturation magnetization, as compared to the parent $CdCr_2Se_4$, indicated changes in the number of competing ferromagnetic and antiferromagnetic interactions. It was thus interesting to study whether the tetrahedral location of Sb is regular for this admixture, and to see an effect of the substitution on magnetic properties in other samples with the Sb concentration, smaller and larger than x=0.25. For these purposes two typical samples with nominal concentration x=0.1 and 0.5 were

E-mail address: ewa.malicka@us.edu.pl (E. Malicka).

0022-4596/$ - see front matter © 2009 Elsevier Inc. All rights reserved.
doi:10.1016/j.jssc.2009.09.002

selected for an X-ray single crystal diffraction in order to determine the location of Sb^{3+} ions in the spinel structure. The magnetic properties were measured using a superconducting quantum interference device (SQUID) magnetometer and the electron spin resonance (ESR) technique was applied to study spin–spin and spin–lattice couplings.

2. Experimental

Single-crystals of the spinel $CdCr_2Se_4$ diluted with antimony atoms were grown from binary selenides CdSe and Sb_2Se_3 by the chemical vapor transport method with anhydrous $CrCl_3$ as a transport agent. Details on the crystal growth were described elsewhere [19].

The chemical composition of the crystals was determined using energy-dispersive X-ray spectrometry (EDXRF). The samples were excited by the air-cooled X-ray tube with Rh target (Oxford Instruments, USA). The X-ray spectra from the samples were collected by thermoelectrically cooled Si-PIN detector (Amptek, USA) with resolution of 145 eV at 5.9 keV. Cadmium, chromium and selenium were determined using $K\alpha$ lines, whereas antimony was identified using $K\beta$ line because Sb $K\alpha$ overlapped with Cd $K\beta$. The quantitative analysis was performed using fundamental parameters method based on the Sherman equation. Pella et al. algorithm was used for the evaluation of X-ray tube spectrum. For the first single-crystal the following composition was obtained: $18.3 \pm 0.4\%$ Cd, $2.97 \pm 0.1\%$ Sb, $20.1 \pm 0.9\%$ Cr, $58.6 \pm 1.6\%$ Se and for second one: $11.7 \pm 0.3\%$ Cd, $10.0 \pm 0.4\%$ Sb, $19.1 \pm 0.8\%$ Cr, $59.2 \pm 1.3\%$ Se.

The single crystal samples, of the dimensions given in Table 1, were selected for X-ray diffraction measurements with graphite monochromated Mo$K\alpha$ radiation using KM-4 Xcalibur single-crystal diffractometer (Oxford Diffraction). The instrument operating in κ geometry was equipped with a CCD detector. The data were collected in ω-scan mode with $\Delta\omega = 1.2^\circ$. About 900 frames were recorded in nine runs with different angular settings, which covered 99% of the Ewald sphere. The exposure time was 28 s/frame. The crystal and instrument stability were monitored through recollecting initial 50 frames at the end of data collection. The diffraction data were integrated for intensities and corrected for Lorentz-polarization effects using the CrysAlis program package [23]. The absorption correction was applied with the Gaussian face-indexed numerical routine [24]. Structure calculations based on F^2 data were made with the SHELXL97 program system [25].

Table 1
Crystal data and experimental details for the spinels $(Cd_{0.87}Sb_{0.13})[Cr_2]Se_4$ and $(Cd_{0.56}Sb_{0.44})[Cr_2]Se_4$.

Structural formula	$(Cd_{0.87}Sb_{0.13})[Cr_2]Se_4$	$(Cd_{0.56}Sb_{0.44})[Cr_2]Se_4$
Space group	$Fd\bar{3}m$ (#227)	$Fd\bar{3}m$ (#227)
Lattice parameters (Å)	10.7364(12)	10.7530(11)
Z	8	8
Density (calculated) (g/cm^3)	5.726	5.737
Crystal size	$0.12 \times 0.12 \times 0.14$	$0.10 \times 0.12 \times 0.14$
Maximum 2θ (deg)	94.47	94.28
Index ranges: h	−22, 12	−22, 13
k	−20, 20	−17, 22
l	−21, 14	−16, 20
Reflections collected	6690	6838
Independent reflections	316	317
Data/parameters	258/10	283/10
Extinction correction	0.00171(9)	0.0019(1)
Final R indices $[I > 2\sigma(I)]$		
R_1; wR_2	2.10; 4.68	2.41; 5.59
Goodness of fit on F^2	0.998	1.002
Minimum and max $\Delta\rho$ (eÅ^{-3})	−2.09, 1.60	−1.81, 1.42

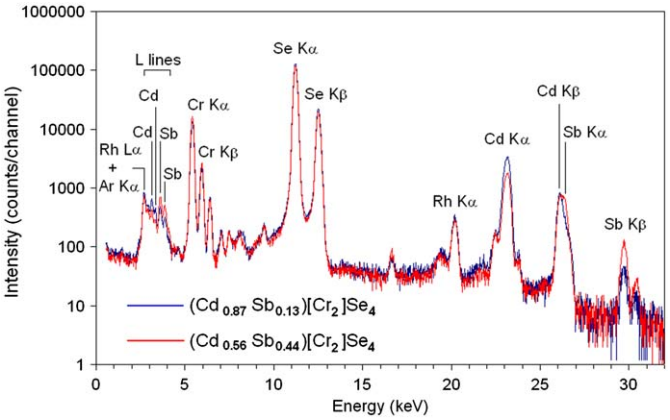

Fig. 1. Energy dispersive X-ray fluorescence spectra (EDXRF) from two analyzed samples of $(Cd_{1-x}Sb_x)[Cr_2]Se_4$.

Magnetic measurements were performed in the temperature range 1.72–400 K and in magnetic fields up to 50 kOe using a Quantum Design MPMS5 SQUID magnetometer. The electron spin resonance spectra were recorded with a standard ESR spectrometer operating at X-band (GHz) frequency using 100 kHz field modulation. The microwave frequency was measured using Hewlett Packard 534 microwave frequency counter. The measurements were performed in the temperature range 90–400 K. The values of ESR parameters, i.e. linewidth (ΔB) and resonance field (B_r), were obtained from the best fit of the simulated Lorenzian profile to the experimentally observed spectra.

3. Results and discussion

The energy dispersive X-ray fluorescence spectra from two analyzed single crystals are given in Fig. 1. It shows that antimony is built into the compounds and the Cd concentration decreases with an increase of Sb concentration.

3.1. Crystal structure and cation distribution

The incorporation of Sb^{3+} ions into the $CdCr_2Se_4$ crystal does not change the cubic symmetry of the compound. The location of Sb dopant was probed both at the tetrahedral (A) and octahedral [B] sites of the spinel structure in the space group $Fd\bar{3}m$ (#227). Since the occupancy factors for two atoms located at the same site are strongly correlated, they cannot be refined simultaneously. Therefore, the site occupancy factors (SOF) for individual cations, treated alternatively as a free parameter, were calculated in consecutive runs with several cycles of the refinement. The first approach, assuming Sb sharing octahedral position with Cr, led to unrealistically large standard deviations on SOF for both the atoms ending with unstable refinement. The same procedure carried out with Sb located in the A-site converged well, thus it was concluded that the Sb^{3+} ions prefer position (A). The chemical formula for the studied quarternary solid solution was accepted to be $(Cd_{1-x}Sb_x)[Cr_2]Se_4$. Several additional cycles of calculations were aimed at checking the anion deficiency, yet no deviations from the stoichiometry were observed.

For spinels with the composition $(A_{0.5}A'_{0.5})[Cr_2]Se_4$, i.e. with two different cations in a ratio 1:1, chemical ordering can be expected that might bring about two different locations of A and A' ions. Within the unit cell of the same dimension, the tetrahedral site order may occur and thus the symmetry may change from the space group $Fd\bar{3}m$ to the non-centrosymmetric space group $F\bar{4}3m$

[26–28]. The lower symmetry would manifest itself in diffraction patterns as an appearance of additional reflections of the {$hk0$} type with $h+k=4n+2$. These reflections are systematically extinct in $Fd\bar{3}m$ but allowed in $F\bar{4}3m$. In the case of the $(Cd_{1-x}Sb_x)[Cr_2]Se_4$ spinels studied in the present work such reflections were totally absent, and hence the lower symmetry and consequently the tetrahedral site ordering were rejected.

The cubic lattice parameter of the parent spinel $CdCr_2Se_4$ is equal to $a=10.736(1)$ Å. With increasing Sb concentration in $(Cd_{1-x}Sb_x)[Cr_2]Se_4$ the unit cell volume was found to increase gradually. For the nominal x values of 0.1, 0.25 and 0.5, the unit cell dimensions are $a=10.7364(12)$, 10.7464(13) [22] and 10.7530(11) Å, respectively. This finding is rather unexpected as the ionic radii of Sb^{3+} and Cd^{2+} are similar (0.74 and 0.78 Å, respectively [29]). Therefore, several additional cycles of calculations were carried out, aimed at checking the anion site. These refinements did not reveal any deviation from the full occupancy.

Table 1 summarizes the crystal data and experimental conditions for two end nominal compositions in the $(Cd_{1-x}Sb_x)[Cr_2]Se_4$ series, i.e., $x=0.1$ and 0.5. The actual dopant concentration derived for these two crystals from the SOF calculations amounts to $x=0.13$ and 0.44. Therefore, the chemical composition of these crystals should be written as $(Cd_{0.87}Sb_{0.13})[Cr_2]Se_4$ and $(Cd_{0.56}Sb_{0.44})[Cr_2]Se_4$, respectively. The results of crystal structure refinements and the interatomic distances in these compounds are given in Tables 2 and 3, respectively.

The Sb^{3+} replacement for Cd^{2+} in the tetrahedral sites of $(Cd_{1-x}Sb_x)[Cr_2]Se_4$ causes an increase of the overall positive charge in the compound, which has to be compensated. Since the selenium anion excess has not been observed, the charge compensation may come throughout the exchange mechanism [30–32], which yields mixed valence of the chromium ions at the octahedral sites $[Cr^{3+}_{2-x}Cr^{2+}_x]$. The assumption of such a charge transfer is consistent with the observation of the systematic increase of the lattice parameter with rising Sb content. As the ionic radii of Cr^{3+} and Cr^{2+} at the [B] sites are 0.615 and 0.73 Å, respectively [29], the appearance of Cr^{2+} ions should result in an expansion of the cubic unit cell of the doped spinels.

Table 2
Fractional atomic coordinates and equivalent isotropic displacement parameters (10^3 Å^2) for (a) $(Cd_{0.87}Sb_{0.13})[Cr_2]Se_4$ and (b) $(Cd_{0.56}Sb_{0.44})[Cr_2]Se_4$.

Atom	Site	Sample (a)		Sample (b)	
		Occupancy	U_{iso}	Occupancy	U_{iso}
Cd	8a (1/8, 1/8, 1/8)	0.0362(1)	7.78(13)	0.0233(1)	9.16(13
Sb	8a (1/8, 1/8, 1/8)	0.0054(1)	7.78(13)	0.0184(1)	9.16(13)
Cr	16d (1/2, 1/2, 1/2)	0.08333	4.52(12)	0.08333	5.24(12)
Se	32e (x, x, x)	0.16667	5.29(9)	0.16667	5.85(9)
		$x=0.26417(2)$		$x=0.26415(2)$	

3.2. Magnetic properties

The magnetic data collected for $(Cd_{0.87}Sb_{0.13})[Cr_2]Se_4$ and $(Cd_{0.56}Sb_{0.44})[Cr_2]Se_4$ are summarized in Figs. 2 and 3, respectively. The measured specimens were single crystals of the two spinels freely placed in sample holders. For both compounds, above room temperature the inverse magnetic susceptibility follows the Curie–Weiss law. The effective magnetic moment μ_{eff}, derived from the fits

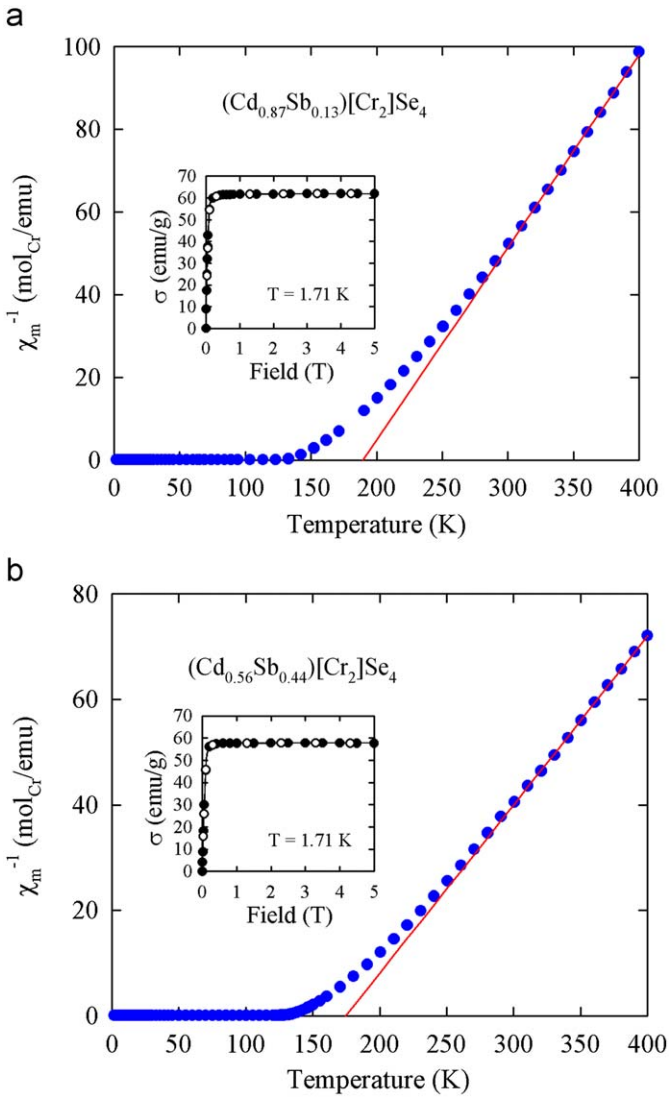

Fig. 2. Temperature dependence of the inverse molar magnetic susceptibility and field variation of the magnetization for (a) $(Cd_{0.87}Sb_{0.13})[Cr_2]Se_4$ and (b) $(Cd_{0.56}Sb_{0.44})[Cr_2]Se_4$. The magnetic susceptibility was measured in a field of 1 kOe, and the magnetization was measured at 1.71 K with increasing (full circles) and decreasing (open circles) field. The solid straight lines are the Curie–Weiss fits discussed in the text.

Table 3
Selected interatomic distances (Å) and angles (deg) for $(Cd_{0.87}Sb_{0.13})[Cr_2]Se_4$ and $(Cd_{0.56}Sb_{0.44})[Cr_2]Se_4$.

Distances	Cd/Sb – Se	Cd/Sb – Cr	Cr – Se	Cr – Cr	Se – Se $_{shortest}$	Se – Se
(a)	2.5880(5)	4.4511(5)	2.5411(3)	3.7959(4)	3.3656(7)	3.8081(4)
(b)	2.5917(5)	4.4580(5)	2.5452(3)	3.8018(4)	3.3712(7)	3.8239(4)
Bond angles	Se – Cd/Sb – Se	Se – Cr – Se	Se – Cr – Se^i			
(a)	109.47(0)	97.06(1)	82.94(1)			
(b)	109.47(0)	96.64(1)	82.95(1)			

Note: The superscript i denotes symmetry operator for generating equivalent atom at $x+\frac{1}{4}$, $y+\frac{1}{4}$, $1-z$.

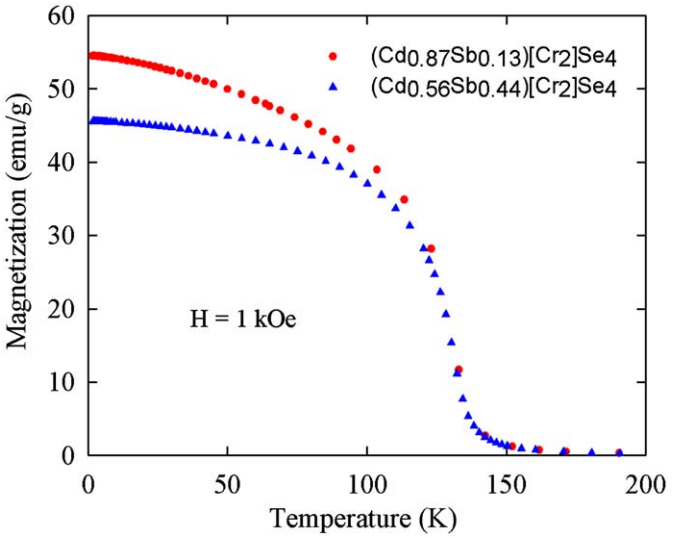

Fig. 3. Temperature dependence of the magnetization in $(Cd_{0.87}Sb_{0.13})[Cr_2]Se_4$ and $(Cd_{0.56}Sb_{0.44})[Cr_2]Se_4$ measured in a field of 1 kOe upon cooling the samples in an applied field.

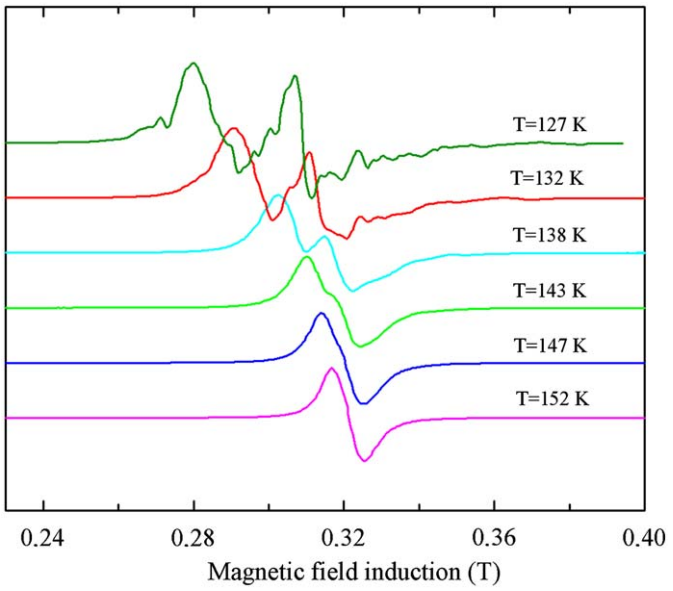

Fig. 4. Temperature dependent evolution of the ESR spectrum for $(Cd_{0.87}Sb_{0.13})[Cr_2]Se_4$.

shown in the figures, amounts to 4.02(5) and 4.21(4) μ_B per Cr atom, respectively. These values should be compared with the spin-only value expected for Cr^{3+} ion that is equal to 3.87 μ_B. The observed difference between the experimental and theoretical values of μ_{eff} results from the charge transfer effect discussed above. The appearance of Cr^{2+} ions, which are characterized by the paramagnetic magnetic moment of 4.90 μ_B, brings about the enhanced magnitude of the experimentally measured moment. From the values of μ_{eff} one may estimate the concentration of Cr^{2+} ions to be 13% and 30% of all the chromium atoms per formula unit in $(Cd_{0.87}Sb_{0.13})[Cr^{2+}_{0.26}Cr^{3+}_{1.74}]Se_4$ and $(Cd_{0.56}Sb_{0.44})[Cr^{2+}_{0.6}Cr^{3+}_{1.4}]Se_4$, respectively. These Cr^{2+} concentrations differ from those derived in the structure calculations, since assuming the cation charge as +8/f.u., they mean a presence of 1.6% and 2% vacancies in $(Cd^{2+}_{0.87}Sb^{3+}_{0.13})[Cr^{2+}_{0.26}Cr^{3+}_{1.74}]Se_4$ and $(Cd^{2+}_{0.56}Sb^{3+}_{0.44})[Cr^{2+}_{0.6}Cr^{3+}_{1.4}]Se_4$, respectively. Location of the vacancies is not clear, but enhanced thermal displacements at the *A*-sites (Table 2), would suggest the tetrahedral sublattice.

The paramagnetic Curie temperature determined for $(Cd_{0.87}Sb_{0.13})[Cr_2]Se_4$ and $(Cd_{0.56}Sb_{0.44})[Cr_2]Se_4$ amounts to 189.6(5) and 175.1(4) K, respectively. These values can be compared with $\theta_p \approx 200$ K reported for pure $CdCr_2Se_4$ [2,4]. The decrease of θ_p with increasing the Sb content may indicate some gradual weakening of the magnetic exchange. This hypothesis seems supported by somewhat less pronounced deviation of the inverse magnetic susceptibility of $(Cd_{0.56}Sb_{0.44})[Cr_2]Se_4$ from the Curie–Weiss law below the room temperature in comparison to that observed for $(Cd_{0.87}Sb_{0.13})[Cr_2]Se_4$ (similarly to the behavior of $CdCr_2Se_4$ [4], this characteristic concave shape of the inverse susceptibility is considered here as a manifestation of short-range magnetic interactions).

As shown in Figs. 2 and 3, both spinels studied order ferromagnetically below 130 K, i.e. at the Curie temperature reported for the parent compound [1,3]. Apparently, the substitution of Sb for Cd does not influence much the long-range magnetic ordering in this system. However, some change is observed in the magnitude of the magnetic moment measured deeply in the ordered state. At 1.71 K, the magnetization saturates in fields stronger than 1 kOe at a value corresponding to 2.95(2) and 2.77(2) μ_B per Cr atom for $(Cd_{0.87}Sb_{0.13})[Cr_2]Se_4$ and $(Cd_{0.56}Sb_{0.44})[Cr_2]Se_4$, respectively.

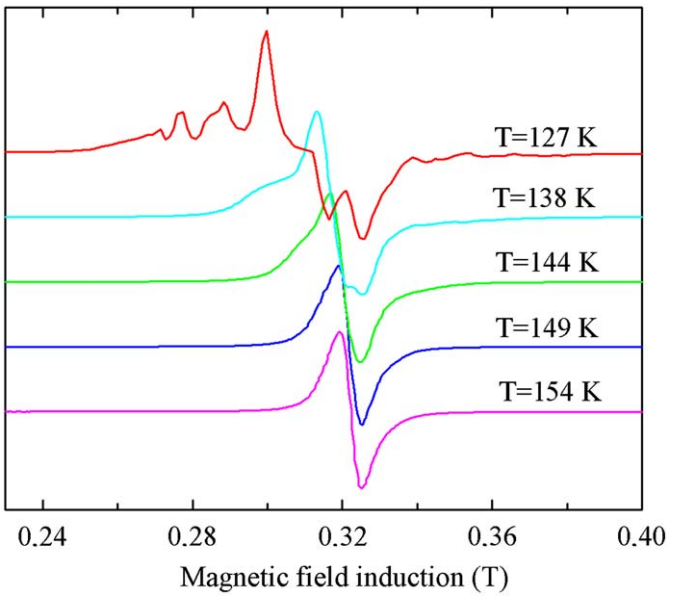

Fig. 5. Temperature dependent evolution of the ESR spectrum for $(Cd_{0.56}Sb_{0.44})[Cr_2]Se_4$.

3.3. ESR data

The electron spin resonance spectra for $(Cd_{0.87}Sb_{0.13})[Cr_2]Se_4$ and $(Cd_{0.56}Sb_{0.44})[Cr_2]Se_4$ measured at various temperatures below 160 K are shown in Figs. 4 and 5, respectively. The spectra exhibit apparently similar behavior. In the paramagnetic region the ESR signal initially consists of a single Lorenzian line with g=1.99, which is attributed to Cr ions. With decreasing temperature towards the ferromagnetic phase transition the signal changes considerably: (a) deviation from the Lorenzian line-shape is observed; (b) the resonance field (B_r) rapidly decreases; (c) the linewidth (ΔB) broadens considerably; (d) the signal intensity strongly increases; (e) the spectra finally split into several features. Moreover, the complexity of the ESR spectrum at the low temperature is related to the structural phase transition

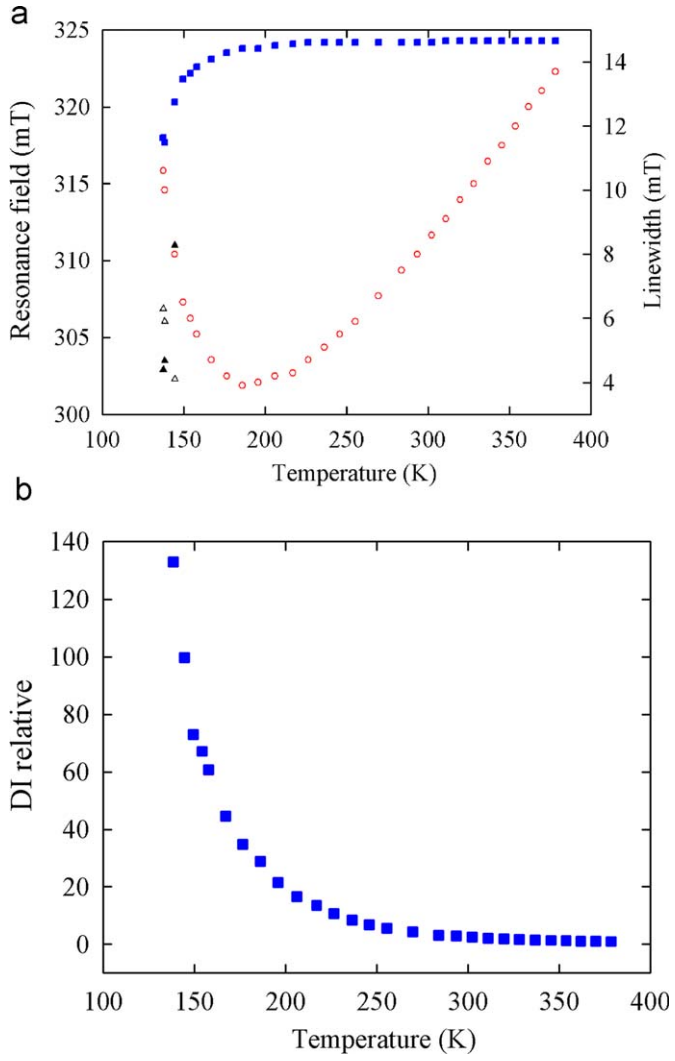

Fig. 6. Temperature variations of the ESR parameters for $(Cd_{0.56}Sb_{0.44})[Cr_2]Se_4$: (a) resonance field and linewidth and (b) double-integrated intensity. Below $T=140$ K the ESR spectrum was fitted to two lines. The corresponding relationship for $(Cd_{0.87}Sb_{0.13})[Cr_2]Se_4$ run the same.

with cubic-to-orthorhombic symmetry change at T_C, taking place in addition to the ferromagnetic transition [22].

The temperature variations of the main ESR characteristics are shown in Fig. 6. Clearly, in the temperature range 400–250 K, the linewidth linearly decreases with decreasing temperature. Generally, the magnitude of ΔB is related to the relaxation processes in spin system, and for individual spin the broadening of the linewith is $\Delta B \sim 1/\tau$, where τ is the spin relaxation time. In a dense magnetic material this relationship is modified, since the magnetization relaxes towards an effective field instead of external field. In this case ΔB can be described as the sum [33,34] $\Delta B = \Delta B_{ss} + \Delta B_{s-ph}$, where the term ΔB_{ss} accounts for magnetic exchange, while ΔB_{s-ph} represents the contribution due to spin–phonon interaction. The magnitude of ΔB_{ss} is defined by the theory of exchange narrowing [35] as $\Delta B_{ss} = [(\Delta B_{dd})^2]/B_{ex}$, where ΔB_{dd} stands for the dipolar-produced linewidth and B_{ex} is the rate of exchange. Within this approach, the linear temperature dependence of the ESR linewidth, observed for both spinels, implies that one-phonon relaxation prevails in the paramagnetic phase even at high temperatures. This effect may be caused by broad phonon bands, which participate in the spin relaxation processes.

With decreasing temperature the exchange interactions become more and more efficient in stimulating a formation of small clusters with short-range magnetic ordering. When approaching the transition temperature T_C, the clusters grow and coalesce to create an infinite magnetic network at T_C. This mechanism explains the observed asymmetry of the ESR lines below about 150 K, as well as the appearance of the new lines below 144 K (see Figs. 4 and 5).

The presence of the short-range magnetic order above T_C manifests itself also in the temperature dependent evolution of the spectrum intensity. The DI values, displayed in Fig. 6b were obtained by double integration of the spectrum. It is expected that DI should be proportional to the spin susceptibility of the sample. As it is apparent from the figures, for both compounds, the DI values increase rapidly below about 200 K. Interestingly, these upturns are even stronger than theoretically predicted for Heisenberg-type ferromagnets, where the magnetic susceptibility should vary as $\chi \approx [(T-T_C)/T_C]^{-p}$ with the exponent $p=4/3$ [36]. The observed behavior may be attributed to the effect of orienting the clusters in external magnetic field.

The spectra measured in the ordered state, i.e. below 130 K, represent ferromagnetic resonance. Their complexity may originate in some inhomogeneity of internal magnetic field. It is known [37–39], that such inhomogeneities arise due to the presence of magnetic domains and/or demagnetization effects in non-spherical samples. As can be seen in Figs. 4–6, the transition region from para- to ferromagnetic state is fairly broad for both compounds. Initially, the paramagnetic signal broadens gradually with decreasing temperature, then shifts from the paramagnetic resonance and finally vanishes in the ordered state. Moreover, from the spectra obtained at 127 K (see Figs. 4 and 5), it may be inferred, that at this temperature still a small fraction of the paramagnetic phase exists in the ferromagnetically ordered lattice. This feature would imply somewhat inhomogeneous nature of the ordered state in the vicinity of T_C.

4. Summary

- The Sb^{3+} ions adopt the tetrahedral location in the cubic centrosymmetric spinel structure of the formula $(Cd_{1-x}Sb_x)[Cr_2]Se_4$. Since the ionic radii of the (A)-site cations are nearly the same, the sensitivity of the unit cell to the admixture concentration suggests the disproportionation of chromium ions in the octahedral sites. The magnetic exchange mechanism leads to the mixed chromium valences Cr^{3+} and Cr^{2+} appearing in order to preserve charge neutrality.
- The tetrahedral location of Sb^{3+} has small impact on magnetic properties of the present compounds. The appearance of Cr^{2+} ions manifests itself in the enhancement of the effective magnetic moment in the mixed spinels $(Cd_{1-x}Sb_x)[Cr_2]Se_4$ with respect to the value reported for the terminal compound $CdCr_2Se_4$. Also the electronic ground state in these spinels as well as short-range interactions in the vicinity of the ferromagnetic phase transition appeared only slightly modified by the Sb^{3+} for Cd^{2+} substitution. The Curie temperature itself remained unaffected by this type of doping, since the Cr–Cr direct interactions and Cr–Se–Cr exchange interactions in the magnetic sublattice turned out not very much sensitive to the lattice turbulences resulting from statistically distributed the Cd and Sb cations in the A-site.
- The short-range interactions persisting above T_C strongly influence the ESR spectra of the $(Cd_{1-x}Sb_x)[Cr_2]Se_4$ spinels. The transition region, dominated by the presence of ferromagnetic clusters appears to be quite broad. Only above 250 K, the ESR linewidth is consistent with the Huber–Seehra theory

derived for magnetically concentrated systems. The observed behavior points to the strong spin–lattice contribution to the magnetic properties of the compounds studied. The temperature dependent evolutions of the ESR spectra suggest that the low temperature phase in both mixed spinels may have non-cubic crystal symmetry.

Acknowledgment

The work was supported by the Ministry of Science and Higher Education by the Grant no. N N204 1784 33 (1784/B/H03/2007/33).

Appendix A. Supplementary materials

The online version of this article contains additional supplementary data. Please visit doi:10.1016/j.jssc.2009.09.002.

References

[1] P.K. Baltzer, P.J. Wojtowicz, M. Robbins, E. Lopatin, Phys. Rev. (1966) 367–377.
[2] P.K. Baltzer, H.W. Lehman, M. Robbins, Phys. Rev. Lett. 15 (1965) 493–495.
[3] H.W. Lehmann, Phys. Rev. 163 (1967) 488–496.
[4] R.C. LeCraw, H. Von Philipsborn, D. Sturge, J. Appl. Phys. 38 (1967) 965–966.
[5] A. Continenza, T. de Pascale, F. Meloni, M. Serra, Phys. Rev. B (1994) 2503–2508.
[6] N. Shanthi, P. Mahadevan, D.D. Sarma, J. Solid State Chem. (2000) 198–205.
[7] V.T. Kalinnikov, T.G. Aminov, V.M. Novotortsev, Neorg. Mater. (2003) 1159–1176;
V.T. Kalinnikov, T.G. Aminov, V.M. Novotortsev, Inorg. Mater. (Engl. Transl.) 39 (2003) 997–1012.
[8] T. Ogasawara, K. Ohgushi, Y. Tomioka, K.S. Takahashi, H. Okamoto, M. Kawasaki, Y. Tokura, Phys. Rev. Lett. 94 (2005) 087202–087214.
[9] C. Haas, A.M.J.G. van Run, P.F. Bongers, W. Albers, Solid State Commun. 5 (1967) 657–661.
[10] A. Amith, L. Friedman, Phys. Rev. B 2 (1970) 434–436.
[11] V.T. Kalinnikov, T.G. Aminov, L.L. Golik, L.N. Novikov, V.A. Zhegalina, N.S. Shumilkin, Izv. Akad. Nauk SSSR Neorg. Mater. 14 (1978) 1408–1412.
[12] L.I. Koroleva, N.P. Pislyakova, T.G. Aminov, G.M. Kuz'micheva, Fiz. Tverd. Tela 32 (1990) 2230–2233.
[13] J.M. Ferreira, M.D. Coutinho-Filho, Phys. Rev. B 54 (1996) 12979–12992.
[14] G.H. Larson, A.W. Sleight, Phys. Lett. 28A (1968) 203–204.
[15] D.A. Tarchov, G.I. Vinogradova, V.G. Veselago, T.K. Menshchikova, G.F. Gubskaya, E.G. Zhukov, Izv. Akad. Nauk SSSR, Neorg. Mater. 30 (1994) 484–488.
[16] I. Okońska-Kozłowska, E. Malicka, A. Waśkowska, J. Heimann, T. Mydlarz, J. Solid State Chem. 158 (2001) 34–39.
[17] T. Groń, A. Krajewski, J. Kusz, E. Malicka, I. Okońska-Kozłowska, A. Waśkowska, Phys. Rev. B 71 (2005) 035208–035209.
[18] G.G. Shabunina, R.A. Sadykov, T.G. Aminov, Neorg. Mater. (2000) 1422–1438;
G.G. Shabunina, R.A. Sadykov, T.G. Aminov, Inorg. Mater. (Engl. Transl.) 36 (2000) 1208–1212.
[19] D. Skrzypek, E. Malicka, A. Waśkowska, S. Widuch, A. Cichoń, T. Mydlarz, J. Cryst. Growth 297 (2006) 419–425.
[20] S.B. Berger, H.L. Pinch, J. Appl. Phys. 38 (1967) 949–950.
[21] A.G. Gurevich, Yu.M. Jakovlev, V.I. Karpovich, A.N. Ageev, E.V. Rubalskaya, Phys. Lett. 40A (1972) 69–70.
[22] A. Waśkowska, L. Gerward, J. Staun Olsen, W. Morgenroth, E. Malicka, D. Skrzypek, J. Phys. Condens. Matter 20 (2008) 1–8 425209.
[23] Oxford Diffraction 2001, CrysAlis CCD. Data Collection software, Wrocław, Poland, Oxford Diffraction Ltd.
[24] Oxford Diffraction 2006, CrysAlis RED, Data Reduction program, Issue 171.32, Oxford Diffraction Ltd.
[25] G.M. Sheldrick, SHELXL-97, Program for Crystal Structure Refinement, University of Gottingen, 1997.
[26] V.N. Zaritskii, R.A. Sadykov, Ya.I. Kostyuk, R.A. Sizov, T.G. Aminov, R.K. Gubaidullin, Sh.R. Safin, Fiz. Tverd. Tela 28 (11) (1986) 3293–3298.
[27] H.D. Lutz, M. Jung, Z. Anorg. Allg. Chem. 579 (1989) 57–60.
[28] H.M. Plamer, C. Geraves, High Temperature Superconductor and Novel Inorganic Materials 62 (1999) 251–256.
[29] R.D. Shanon, Acta Crystallogr. A32 (1976) 751–767.
[30] C. Zener, Phys. Rev. 82 (1951) 403–405.
[31] P.W. Anderson, H. Hasegawa, Phys. Rev. 100 (1955) 675–681.
[32] P.G. de Gennes, Phys. Rev. 118 (1960) 141–154.
[33] D.L. Huber, M.S. Seehra, J. Phys. Chem. Solids 36 (1975) 723–725.
[34] M.S. Seehra, M.M. Ibrahim, V.S. Babu, G. Srinivasan, J. Phys. Condens. Matter 8 (1996) 11283–11289.
[35] A. Abragam, B. Bleaney, Electron Paramagnetic Resonance of Transition Ions, Clarendon Press, Oxford, 1970.
[36] W. Zarek, Acta Phys. Pol. A52 (1977) 657–663 and references therein.
[37] C. Kittel, Phys. Rev. 73 (1948) 155;
C. Kittel, Phys. Rev. 76 (1949) 743.
[38] D.S. Schmool, J.M. Barandiaran, J. Magn. Magn. Mater. 191 (1999) 211–224.
[39] R. Szymczak, A. Szewczyk, M. Baran, V. Tsurkan, J. Magn. Magn. Mater. 88 (1990) 481–482.